Electronic Journal of Biotechnology 83 (2026) 100723

Contents lists available at ScienceDirect

Electronic Journal of Biotechnology

journal homepage: www.elsevier.com/locate/ejbt

Research article

IGF2BP3 promotes diabetic retinopathy development by enhancing SEMA3G mRNA stability ☆

You Chen *, Tong Zhao, MengYu Han, Yi Chen

Department of Ophthalmology, China-Japan Friendship Hospital, Chaoyang District, Beijing City, China

GRAPHICAL ABSTRACT

IGF2BP3 promotes diabetic retinopathy development by enhancing SEMA3G mRNA stability.

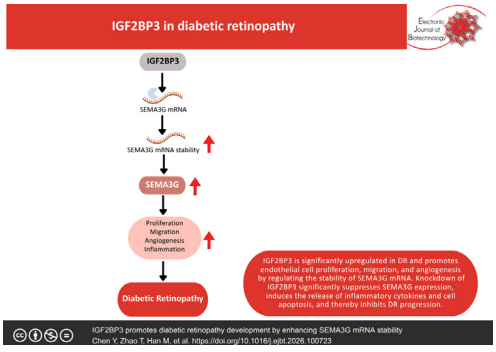

ARTICLE INFO

Article history:
Received 27 January 2026
Accepted 28 April 2026
Available online 15 July 2026

Keywords:
Angiogenesis
Cell proliferation
Cytokines
Diabetic retinopathy
Gene regulation
IGF2BP3
Inflammation
Microvascular proliferation
mRNA stability
Retinal pathology
SEMA3G

ABSTRACT

Background: Diabetic retinopathy is characterized by excessive microvascular proliferation that leads to vitreous hemorrhage, retinal traction, and subsequent visual impairment. Aberrant expression of IGF2BP3 is involved in the pathogenesis of multiple diseases. This study aimed to elucidate the mechanism by which IGF2BP3 mediates diabetic retinopathy by regulating semaphorin-3G (SEMA3G) expression.
Results: Elevated IGF2BP3 expression was observed in diabetic retinopathy. *In vitro*, IGF2BP3 overexpression promoted pathological angiogenesis, whereas its knockdown significantly attenuated wound healing, reduced inflammatory cytokine secretion, and suppressed cellular proliferation. A targeted regulatory relationship between IGF2BP3 and SEMA3G mRNA was identified, with IGF2BP3 enhancing SEMA3G mRNA stability. SEMA3G was upregulated in diabetic retinopathy, and its overexpression partially rescued the diabetic retinopathy progression suppressed by IGF2BP3 silencing. *In vivo*, IGF2BP3 overexpression aggravated histopathological alterations, thereby accelerating diabetic retinopathy development.
Conclusions: In summary, IGF2BP3 promotes diabetic retinopathy development by enhancing SEMA3G mRNA stability.
How to cite: Chen Y, Zhao T, Han M, et al. IGF2BP3 promotes diabetic retinopathy development by enhancing SEMA3G mRNA stability. Electron J Biotechnol 2026;83. https://doi.org/10.1016/j.ejbt.2026.100723.

☆ Audio abstract available in Supplementary material.
Peer review under responsibility of Pontificia Universidad Católica de Valparaíso.
* Corresponding author.
E-mail address: chenyoudt@163.com (Y. Chen).

https://doi.org/10.1016/j.ejbt.2026.100723
0717-3458/

1. Introduction

According to the 11th edition of the International Diabetes Federation (IDF) Diabetes Atlas, the number of adults with diabetes aged 20–79 years worldwide reached 589 million in 2024, accounting for 11.1% of the global population in this age group. Without effective intervention, diabetes is projected to affect nearly 900 million people globally by 2050, and the prevalence is projected to rise to 12.96% [1,2]. As the patient population expands rapidly, the number of individuals with diabetic microvascular complications is expected to increase correspondingly. Among working-age populations, diabetic retinopathy (DR) has emerged as the leading cause of blindness and vision impairment [3]. DR not only results in irreversible vision loss and reduced quality of life for patients but also imposes a substantial socioeconomic burden. DR is primarily characterized by heightened retinal vascular permeability, dysfunction in retinal microvascular endothelial cells, abnormal cell proliferation, and an elevated release of pro-angiogenic factors, all of which occur under prolonged hyperglycemic conditions. These pathological alterations result in excessive and disorganized microvasculature within the retina [4]. The development of DR is closely associated with the aberrant behaviors of human retinal microvascular endothelial cells (HRMECs), including excessive migration, proliferation, and angiogenesis [5]. Pathological angiogenesis is a key indicator of disease progression, marking the transition from early non-proliferative DR to the more advanced proliferative stage [5]. This uncontrolled vascular growth disrupts the integrity of both endothelial cells and blood vessels, leading to irregular vessel architecture, hemodynamic instability, vitreous hemorrhage, and tractional retinal detachment, all of which contribute to severe vision loss [6]. Consequently, the restoration of endothelial function and the inhibition of pathological retinal neovascularization continue to be crucial therapeutic objectives in the management of DR [7].

Recent years have witnessed growing interest in the role of RNA-binding proteins (RBPs) in disease development. Insulin-like Growth Factor 2 mRNA-Binding Protein 3 (IGF2BP3), an inflammation-associated RBP, modulates gene expression by regulating RNA transport and stability [8]. Previous studies have indicated that IGF2BP3 expression is significantly elevated in retinal pigment epithelial (RPE) cells under high glucose (HG) conditions. Mechanistically, the long non-coding RNA Metastasis-Associated Lung Adenocarcinoma Transcript 1 exacerbates HG-induced RPE cell damage by upregulating IGF2BP3 expression, thereby activating the Nuclear Factor Kappa B signaling pathway [9]. However, the specific role of IGF2BP3 in microvascular endothelial cells in DR remains to be fully elucidated.

A growing body of research has demonstrated that the physiological and pathological processes of the vascular system are extensively regulated by semaphorin signaling pathways [10]. SEMA3G, a member of the class 3 semaphorin (Sema3) family, is primarily expressed and secreted by endothelial cells and has been implicated in neuronal development, angiogenesis, and tumor progression [11–13]. Previous studies have shown that endothelial-specific knockdown of SEMA3G in mice with ischemic retinopathy reduces vascular density, accelerates excessive matrix deposition, and decreases pericyte recruitment, suggesting that SEMA3G regulates vascular stability [14]. In mouse models with inhibited or overactivated Notch signaling, SEMA3G promotes orderly vascular regeneration [15]. Furthermore, endothelial-derived SEMA3G promotes the proliferation and migration of human aortic smooth muscle cells by activating YAP signaling, thereby accelerating intimal hyperplasia in diabetic patients [16]. These findings highlight the critical role of SEMA3G in vascular development and pathology; however, its specific function in endothelial cells during DR remains unclear.

IGF2BP3, as an RNA-binding protein, has a known function in stabilizing target mRNAs. Given that bioinformatic predictions indicate the presence of potential IGF2BP3 binding sites in the 3′ untranslated region (3′UTR) of SEMA3G mRNA, it was hypothesized that during the progression of DR under high glucose conditions, IGF2BP3 may drive abnormal retinal microvascular proliferation by binding to and regulating the stability of SEMA3G mRNA. Therefore, this study investigates the role of IGF2BP3 in DR pathogenesis, particularly its regulatory effects on DR progression through stabilizing semaphorin-3G (SEMA3G) mRNA. By elucidating the molecular mechanisms of the IGF2BP3-SEMA3G axis in DR, this work may provide novel diagnostic and therapeutic strategies for early-stage DR intervention.

2. Materials and methods

2.1. Human tissue sample collection

From 2021 to 2024, a total of 60 patients were enrolled from China-Japan Friendship Hospital, and written informed consent was obtained from all participants. The study was approved by the Institutional Review Board of China-Japan Friendship Hospital (2020-12-K09). Vitreous humor samples were collected from 30 patients clinically diagnosed with proliferative vitreoretinopathy (experimental group) and 30 patients with idiopathic macular hole (control group). During vitreous humor collection, the perfusion system was maintained in a closed configuration. The collection protocol involved sequential steps: (1) removal of the vitreous cutter cap, (2) attachment of a sterile 5 mL syringe, and (3) controlled aspiration of vitreous fluid. Immediately following extraction, specimens were flash-frozen in liquid nitrogen and maintained at −80°C for preservation. Following exclusion of unusable samples (e.g., those from patients who received anti-vascular endothelial growth factor (VEGF) therapy within 3 months or had a volume of less than 1.5 mL), 20 paired samples were ultimately selected for subsequent experiments [9].

2.2. Quantitative real-time polymerase chain reaction (RT-qPCR)

Retinal tissues were collected from mouse models, and total RNA was isolated from both the tissues and cultured cells using TRIzol reagent (Invitrogen, MA, USA), following the manufacturer's instructions. The isolated RNA was then reverse-transcribed into cDNA using a reverse transcription kit provided by Sevenbio (Beijing, China). RT-qPCR was performed with SYBR Green Master Mix (Roche, Beijing, China) to analyze gene expression. The relative mRNA levels of target genes were calculated using the $2^{-\Delta\Delta Ct}$ method. Primer sequences used for RT-qPCR analysis are listed in Table 1.

Table 1
Primer sequences for RT-qPCR.

Genes	Primer sequence (5′-3′)
IGF2BP3 (Mus)	F: 5′-GAGGCGCTTTCAGGTAAAATAGAATGA-3′
	R: 5′-AATGAGGCGGGATATTTCGTAT-3′
GAPDH (Homo)	F: 5′-TGCAACCGGGAAGGAAATGA-3′
	R: 5′-TGATGGCATGGACTGTGGTC-3′
GAPDH (Mus)	F: 5′-GCCTCCTCCAATTCAACCCT-3′
	R: 5′-CTCGTGGTTCACACCCATCA-3′
Sema3G (Mus)	F: 5′-GCCAGAGCCAAAACAAAGCAG-3′
	R: 5′-AGTGTAGTTTCCTGCGTCATGG-3′
Sema3G (Homo)	F: 5′-CTCAAAGTCATCGCTCTCCAGGC-3′
	R: 5′-AGTGCCGTAAGTCTCACATTGG'
IGF2BP3 (Homo)	F: 5′-TATATCGGAAACCTCAGCGAGA-3′
	R: 5′-GGACCGAGTGCTCAACTTCT-3′

2.3. Western blot

Total protein was extracted from murine retinal tissues using a protein extraction kit (Solarbio Biotech, Beijing, China). Protein concentrations were determined using a bicinchoninic acid assay kit (Solarbio Biotech). For Western blot analysis, 20 μg of protein from each sample was separated by 10% sodium dodecyl sulfate–polyacrylamide gel electrophoresis (SDS-PAGE) and then transferred onto polyvinylidene fluoride membranes (Millipore, MA, USA) at 4°C. The membranes were blocked with 5% bovine serum albumin (Sangon Biotech, Shanghai, China) for 1 h at room temperature, followed by overnight incubation with primary antibodies at 4°C. Afterward, horseradish peroxidase (HRP)-conjugated secondary antibodies (Thermo Fisher Scientific, Shanghai, China; #61-6520) were applied and incubated for 1 h at 37°C. Protein bands were visualized using an ultrasensitive enhanced chemiluminescence detection reagent (Yeasen Biotech, Shanghai, China) and captured with an ImageQuant LAS system (GE Healthcare) [7]. GAPDH served as the loading control. The specific primary antibodies used in the Western blot analysis are listed in Table 2.

2.4. Cell culture

HRMECs obtained from Shanghai Qida Biotechnology Co., Ltd. (Shanghai, China) were cultured using endothelial cell medium provided by ScienCell (CA, USA). This medium was enriched with essential and non-essential amino acids, vitamins, organic and inorganic compounds, hormones, growth factors, trace minerals, and supplemented with 5% fetal bovine serum. The cell cultures were maintained in a bicarbonate-buffered system at 37°C in an atmosphere of 5% CO_2 and 95% humidity. The pH was maintained at 7.4. The experimental setup involved two distinct groups: (1) the control group, which was cultured in endothelial medium supplemented with 5.5 mmol/L glucose, and (2) the HG group, which was cultured in endothelial medium supplemented with 30 mmol/L glucose.

2.5. Cell transfection

IGF2BP3 and SEMA3G siRNA and the corresponding negative control (si-NC) were procured from Genepharma, located in Suzhou, China. Additionally, the IGF2BP3 overexpression plasmid (OE-IGF2BP3), its negative control (OE-NC), and the SEMA3G overexpression plasmid (OE-SEMA3G) were acquired from RiboBio (Guangzhou, China). These vectors were transiently introduced into HRMECs utilizing the Lipofectamine 2000 transfection reagent (Invitrogen). The cells were subsequently harvested 48 h following transfection, and the efficiency of transfection was assessed by RT-qPCR and Western blot analysis. The siRNA sequences were as follows: (si-IGF2BP3): 5′-GGGAGTCTTATGAAAATGATATT-3′; (si-SEMA3G): 5′-CCCCTTTGACCATGTAATAAATG-3′; and (si-NC): 5′-CACGTGTAAATGTAACCTATTCC-3′.

2.6. Cell counting kit-8 (CCK-8) assay

Cell proliferation was assessed using a CCK-8 assay kit (Sevenbio). Cells were seeded in 96-well plates at a density of 1×10^3 cells per well. CCK-8 reagent (10 μL per well) was added at 24, 48, and 72 h. After 2 h of incubation, the optical density was measured at 450 nm using a microplate reader (Bio-Rad, CA, USA).

Table 2
Primary antibodies for Western blot.

Antibody name	Dilutions	Vendor name	Cat No.
IGF2BP3	1:1000	Thermo Fisher Scientific	MA5-27484
SEMA3G	1:2000	Abmart	MG751394
CD31	1:1000	Thermo Fisher Scientific	MA5-60706
VEGFA	1:1000	Thermo Fisher Scientific	MA5-13182
Cyclin D1	1:3000	Proteintech	60186-1-Ig
GAPDH	1:10000	Proteintech	60004-1-Ig

2.7. 5-Ethynyl-2′-deoxyuridine (EdU) assay

To assess cellular proliferation, HRMECs were plated in 6-well culture dishes at a density of 4×10^3 cells per well following transfection. The EdU assay (Beyotime, Shanghai) was performed according to the manufacturer's specifications. Cells were exposed to 10 μM EdU solution for 2 h under standard culture conditions (37°C, 5% CO_2). Subsequent processing involved dual staining: proliferating cells were identified using Alexa Fluor 488-conjugated azide (Merck, Shanghai) which emits green fluorescence, while nuclear counterstaining was achieved with Hoechst 33342 dye (Yeasen Biotech), producing blue fluorescence. Quantitative analysis of proliferation rates was conducted by determining the percentage of EdU-incorporated (green fluorescent) cells relative to the total cell population identified by nuclear staining. Fluorescent images were acquired using an inverted fluorescence microscope.

2.8. Wound healing assay

For the wound healing assay, HRMEC monolayers were established by plating 7×10^4 cells per well in 6-well culture plates. When cultures attained 90% confluency, uniform linear wounds were generated across the cell monolayer using sterile 200 μL pipette tips. Following wound creation, cellular debris was eliminated through three gentle washes with phosphate-buffered saline (Beyotime). The migration process was documented by acquiring phase-contrast images immediately after wounding (0 h) and after 24 h of incubation using an inverted microscope (Olympus, PA, USA). Three randomly selected fields were analyzed by measuring the gap distance at 24 h, normalized to the initial wound width.

2.9. Angiogenesis assay

A 50 μL aliquot of Matrigel (Corning, NY, USA) was added to each well of a 96-well plate and polymerized at 37°C for 1 h. Subsequently, 2×10^5 cells were seeded per well and incubated at 37°C. Tube formation was observed and photographed under an inverted microscope after 4–6 h.

2.10. Enzyme-linked immunosorbent assay (ELISA) detection

To analyze inflammatory mediators and IGF2BP3 expression, conditioned media from HRMEC cultures were harvested and frozen at –80°C prior to analysis. The secretion profiles of key inflammatory markers, including tumor necrosis factor-alpha (TNF-α), interleukin-1 beta (IL-1β), interleukin-6 (IL-6), and monocyte chemoattractant protein-1 (MCP-1), were determined through enzyme-linked immunosorbent assays employing commercially available kits (R&D Systems, MN, USA). Simultaneously, vitreous IGF2BP3 concentrations were assessed using a specialized human ELISA assay (KAKXBIO, Shanghai, China; KKX-15887R), with all procedures strictly following the manufacturers' protocols. Optical density measurements for all ELISA reactions were obtained using a Multiskan FC spectrophotometric plate reader (Thermo Fisher Scientific).

2.11. Flow cytometry apoptosis assay

Cell apoptosis was analyzed using an Annexin phycoerythrin-fluorescein isothiocyanate (V-FITC)/propidium iodide (PI) apoptosis detection kit (BestBio, Shanghai, China) following the manufacturer's protocol. Cells were resuspended in a binding buffer at a

density of 1×10^6 cells/mL and stained with Annexin V-FITC (Merck, Darmstadt, Germany) and PI (Merck) for 20 min at room temperature in the dark. Apoptotic rates were quantified by flow cytometry (BD Biosciences, CA, USA) [14].

2.12. mRNA half-life

HRMECs were treated with 5 μM actinomycin D (ActD; Sigma-Aldrich, MO, USA) for 0, 2, 4, 6, and 8 h. Total RNA was then extracted and reverse transcribed into cDNA. Relative RNA levels at each time point were normalized to baseline (0 h). mRNA decay kinetics were analyzed using a one-phase exponential decay model (GraphPad Prism software).

2.13. RNA immunoprecipitation (RIP)

RIP was performed using the EZ-Magna RIP Kit (Merck, Millipore; #17-700). Briefly, HRMEC lysates were prepared with lysis buffer and incubated with magnetic beads conjugated to specific antibodies (IGF2BP3 and normal immunoglobulin G [IgG] control) at 4°C overnight. Immune complexes were digested with Proteinase K (Solarbio Biotech), followed by RNA extraction and RT-qPCR to determine SEMA3G mRNA enrichment [17]. Primary antibodies used for RIP are listed in Table 3.

2.14. Construction of animal models

All animal experiments were carried out following protocols approved by the Animal Care and Use Committee of China-Japan Friendship Hospital (ZRDWLL240055). A total of 100 male C57BL/6J mice, aged 6 weeks, were obtained from Shanghai SLAC Laboratory Animal Co., Ltd. (Shanghai, China) and allowed to acclimatize for one week under controlled environmental conditions (22 ± 2°C, 55 ± 5% humidity, 12-h light/dark cycle, and 15–20 air changes per hour). After a 12-h fasting period, diabetes was induced by intraperitoneal injection of streptozotocin (60 mg/kg/-day in 0.1 M citrate buffer, pH 4.5) for five consecutive days. Diabetic mice with fasting blood glucose ≥ 16.7 mmol/L (tail vein blood sampling at 4 weeks post-injection) were included. Control mice received an equivalent volume of citrate buffer. Thirty mice served as normal control group, while 30 diabetic mice were divided into early-DR (15 mice, sampled at 12 weeks of age) and the late DR group (15 mice, sampled at 24 weeks of age). Forty additional diabetic mice were randomly assigned to four treatment groups (n = 10/group): AAV-sh-NC, AAV-sh-IGF2BP3, AAV-oe-NC, or AAV-oe-IGF2BP3. Adeno-associated viruses (AAVs) carrying the IGF2BP3 overexpression plasmid (oe-IGF2BP3) and control plasmid (oe-NC), as well as the IGF2BP3 knockdown plasmid (IGF2BP3-shRNA: 5′-CAACAAGATGAAGAGCACCA-3′) and negative control (shNC: 5′-GCAGAAGATGAAGAAGAATAT-3′), were purchased from RiboBio (Guangzhou, China). Viral vectors (Thermo Fisher Scientific) were delivered by intravitreal injection under anesthesia with 2,2,2-tribromoethanol (10 mL/kg, intraperitoneally). Following pupil dilation with 0.5% atropine, 1.5 μL viral suspension (1×10^{12} vg/mL, AAV2/9) was injected 1.5 mm posterior to the corneal limbus using a 33-gauge Hamilton syringe. Antibiotic ointment was applied postoperatively. At 24 weeks, enucleated eyes were fixed in 4% paraformaldehyde for analysis.

Table 3
Primary antibodies for RIP.

Antibody name	Vendor name	Cat No.
IGF2BP3	Thermo Fisher Scientific	PA5-96506
IgG	Thermo Fisher Scientific	MA5-42729

2.15. Immunofluorescence staining

Mouse eyeballs were paraffin-embedded and sectioned at 4-μm thickness. Sections were dehydrated in 95% ethanol for 10 min and then incubated with 10% serum (TIANDZ, Beijing, China) for 30 min. After removing the serum, sections were incubated with primary antibody against IGF2BP3 (Thermo Fisher Scientific; MA5-27484) and Alexa Fluor™ 488-conjugated secondary antibody (Thermo Fisher Scientific; A-11008). Nuclei were counterstained with 4′,6-diamidino-2-phenylindole (Sewenbio, Beijing, China), and images were acquired using a fluorescence microscope (Olympus).

2.16. Immunohistochemistry

Fresh retinal tissues from C57BL/6J mice were fixed in 4% paraformaldehyde, dehydrated through a graded ethanol series, and paraffin-embedded. Tissue sections were incubated with a primary antibody against IGF2BP3 (Thermo Fisher Scientific, MA5-27484) at 4°C overnight, followed by incubation with an HRP-conjugated secondary antibody (Goat anti-Rabbit IgG (H + L), Thermo Fisher Scientific; #31460) at room temperature for 1 h. Sections were then treated with Vectastain Elite ABC reagent (Vector Laboratories, USA) for 30 min. After color development with 3,3′-diaminobenzidine (Solarbio Biotech), tissues were counterstained with hematoxylin (Solarbio Biotech) and examined under a microscope (Leica, Wetzlar, Germany).

2.17. Histological examination of mouse retina by hematoxylin-eosin (HE) staining

Mouse retinal tissues were processed for paraffin sectioning. Eyeballs were initially immersed in Formalin-Acetic Acid-Alcohol (FAA fixative; Jingke Chemical, Shanghai, China) for 1 min, followed by fixation in 10% neutral buffered formalin. Tissues were dehydrated through 95% ethanol for 10 min, cleared in xylene (3–4 min), and embedded in paraffin at 60°C for 2 h. Sections (4-μm thickness) were baked at 65°C for 1 h. The staining protocol included hematoxylin (Yulu Experiment Equipment, Jiangxi, China; 15 min), differentiation in 1% acid-alcohol (1–2 min), treatment with 1% ammonium hydroxide (8–10 s), and eosin counterstaining (Yulu Experiment Equipment; 1 min). After standard dehydration and mounting, retinal histopathology was examined under a light microscope (Leica) [18].

2.18. Data analysis

Data were analyzed using GraphPad Prism software. Results are expressed as mean ± standard deviation. Intergroup comparisons were performed using Student's *t*-test or analysis of variance. A p value < 0.05 was considered statistically significant.

3. Results

3.1. Elevated expression of IGF2BP3 in DR

ELISA demonstrated a notable increase in IGF2BP3 protein levels within the vitreous humor of patients diagnosed with DR (Fig. 1A). However, this significant upregulation was not observed in mice at the early stage of DR (Fig. 1B). Complementary findings from western blot analysis further verified a significant elevation of IGF2BP3 protein expression in late-stage DR mice when compared to the control group (Fig. 1C). Similarly, both immunofluorescence and immunohistochemistry analyses indicated pronounced IGF2BP3 expression in retinal tissues of the late-stage DR group relative to controls (Fig. 1D, E). In addition,

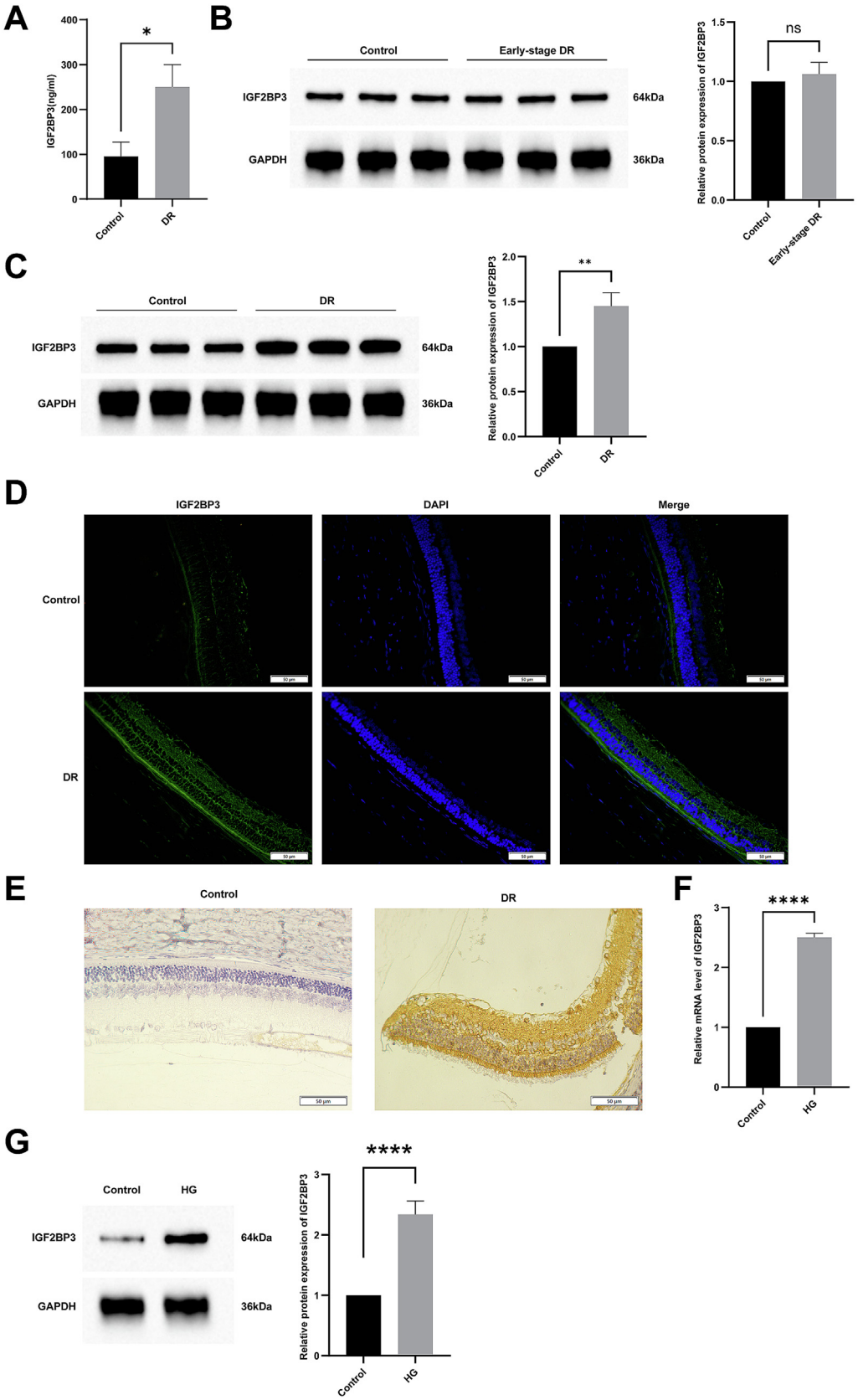

Fig. 1. Elevated expression of IGF2BP3 in DR. (A) ELISA detection of IGF2BP3 protein levels in samples from DR and non-DR patients; (B) Western blot analysis of IGF2BP3 expression in control versus early-stage DR mice; (C) Western blot analysis of IGF2BP3 protein expression in control versus late-stage DR mice; (D) Immunofluorescence staining of IGF2BP3 in control and late-stage DR mice. Scale bar: 50 μm; (E) Immunohistochemical staining of IGF2BP3 in control and late-stage DR mice. Scale bar: 50 μm; (F) RT-qPCR analysis of differential IGF2BP3 mRNA expression at the cellular level; (G) Western blot analysis of differential IGF2BP3 protein expression at the cellular level. Error bars represent the mean ± SEM. * $p < 0.05$; ** $p < 0.01$; **** $p < 0.0001$; ns, not significant.

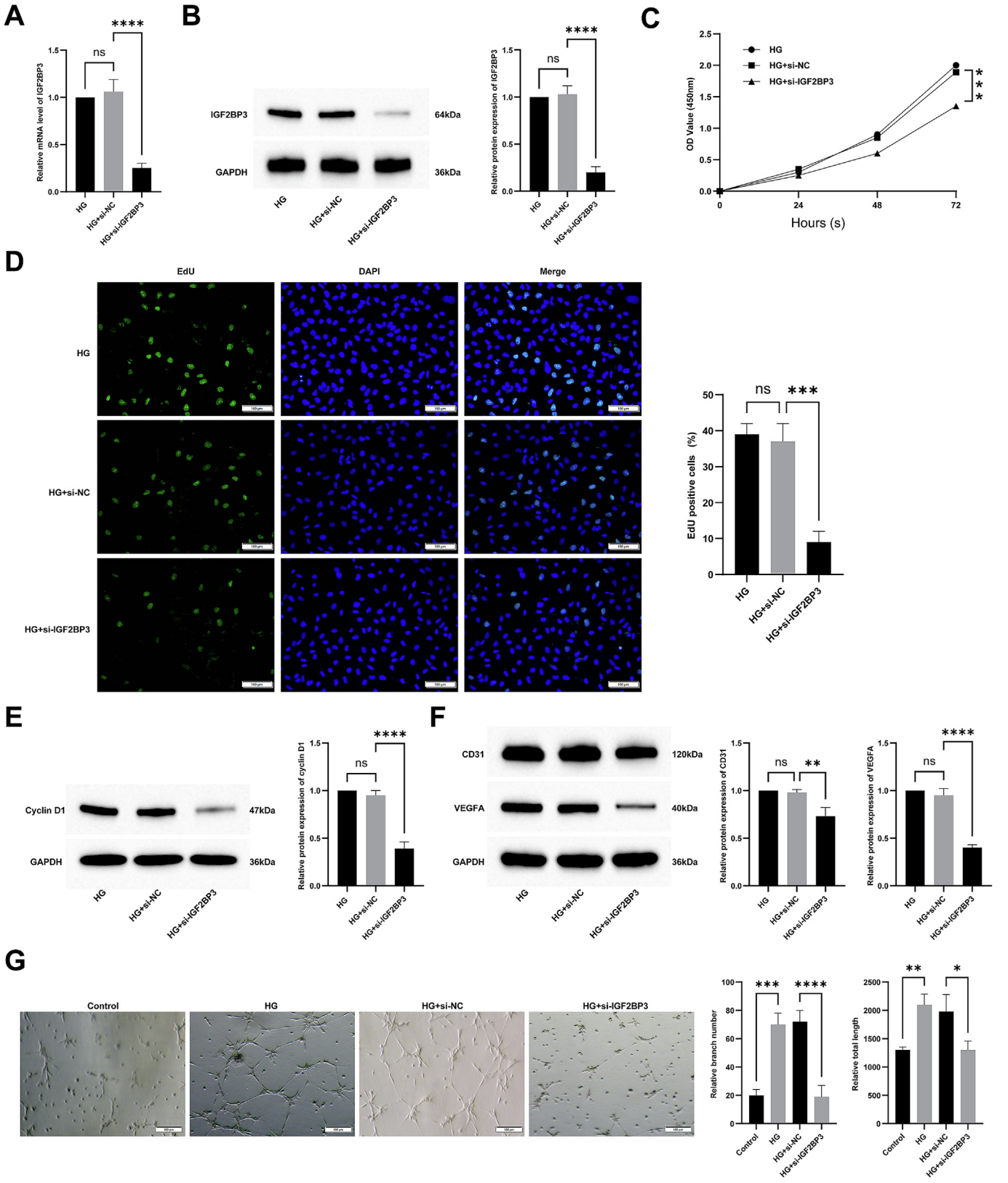

Fig. 2. The effects of IGF2BP3 on cell proliferation and angiogenesis. (A) RT-qPCR analysis of IGF2BP3 transfection efficiency; (B) Western blot analysis of IGF2BP3 transfection efficiency; (C) CCK-8 assay measuring the effect of si-IGF2BP3 on cell proliferation; (D) EdU assay evaluating the effect of si-IGF2BP3 on cell proliferation. Scale bar: 100 μm; (E) Western blot analysis of cyclin D1 protein levels after si-IGF2BP3 transfection; (F) Western blot analysis of CD31 and VEGFA protein levels following si-IGF2BP3 transfection; (G) Tube formation assay assessing the effects of HG and si-IGF2BP3 on HRMEC angiogenic capacity. Scale bar: 100 μm. Error bars represent the mean ± SEM. * $p < 0.05$; ** $p < 0.01$; *** $p < 0.001$; **** $p < 0.0001$; ns, not significant.

increased levels of IGF2BP3 mRNA and protein were detected in a DR cell model (Fig. 1F, G). Together, these findings indicate that IGF2BP3 is substantially upregulated during DR progression and is particularly prominent at advanced stages of the disease.

3.2. Knockdown of IGF2BP3 suppresses retinal angiogenesis in vitro

To elucidate the molecular mechanisms underlying DR, an HG-induced injury model was established using HRMECs. The effective knockdown of IGF2BP3 was confirmed via RT-qPCR and Western blot analysis (Fig. 2A, B). Cell proliferation was assessed using the CCK-8 assay and EdU incorporation. Results from the CCK-8 assay revealed a significant reduction in cell proliferation following IGF2BP3 silencing (Fig. 2C), a finding corroborated by EdU staining, which demonstrated a decreased proportion of EdU-positive cells and reduced proliferative capacity (Fig. 2D). Furthermore, the expression of cyclin D1, a critical regulator of cell cycle progression, was markedly downregulated in IGF2BP3-deficient cells (Fig. 2E). These findings suggest that IGF2BP3 suppression impairs HRMEC proliferation under high-glucose conditions. Considering the pivotal role of angiogenesis in the pathogenesis of DR, further investigations were conducted to evaluate the impact of IGF2BP3 on angiogenic activity. Results showed that the expression of angiogenesis-associated markers, including CD31 and vascular endothelial growth factor A (VEGFA), was notably decreased in IGF2BP3-deficient cells (Fig. 2F). Tube formation assays revealed a significant impairment in angiogenic capacity in HRMECs treated with si-IGF2BP3 when compared to control groups (Fig. 2G). These findings collectively support the notion that IGF2BP3 positively regulates angiogenesis in HRMECs and may contribute to DR development.

3.3. Knockdown of IGF2BP3 impairs wound healing, attenuates inflammatory cytokines, and enhances apoptosis

The effects of IGF2BP3 modulation on HRMEC cell motility, inflammatory responses, and apoptotic activity were investigated using comprehensive *in vitro* analyses. Wound closure assays demonstrated significantly attenuated migratory capacity in IGF2BP3-deficient cells (si-IGF2BP3) relative to control groups after 24 h of observation (Fig. 3A). Subsequent evaluation of inflammatory mediators revealed substantial downregulation of critical cytokines (TNF-α, IL-1β, IL-6, and MCP-1) in IGF2BP3-silenced populations (Fig. 3B). Flow cytometric quantification of apoptotic indices further showed elevated programmed cell death rates following IGF2BP3 depletion (Fig. 3C). These coordinated observations imply that genetic inhibition of IGF2BP3 may exert therapeutic effects against DR pathogenesis through multiple mechanisms: inhibition of endothelial cell motility, attenuation of pro-inflammatory signaling, and enhancement of apoptotic pathways.

3.4. Elevated SEMA3G expression in DR mediated by IGF2BP3-dependent mRNA stabilization

To investigate the molecular mechanism of IGF2BP3 in DR, potential target genes of IGF2BP3 were predicted using the bioinformatics database StarBase 3.0 (https://rnasysu.com/encori/). The results indicated that IGF2BP3 might specifically bind to the 3′UTR of SEMA3G mRNA (Fig. 4A). RIP assays confirmed the binding between IGF2BP3 and SEMA3G mRNA (Fig. 4B, Fig. S1A). Furthermore, mRNA stability assays using ActD treatment in HRMECs demonstrated that SEMA3G mRNA stability was

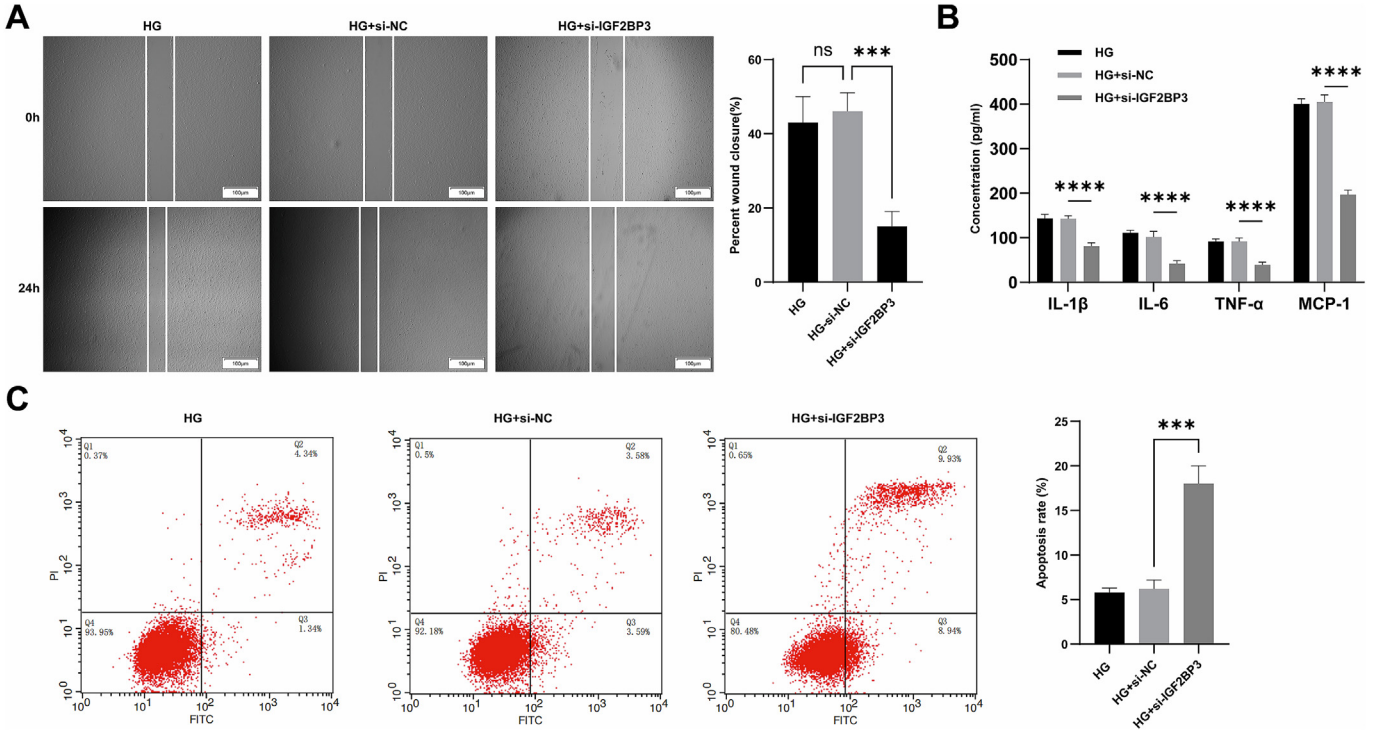

Fig. 3. Knockdown of IGF2BP3 impairs wound healing, attenuates inflammatory cytokines, and enhances apoptosis. (A) Wound healing assay assessing cell migration capacity after si-IGF2BP3 treatment. Scale bar: 100 μm; (B) ELISA measurement of TNF-α, IL-1β, IL-6, and MCP-1 levels; (C) Flow cytometry analysis of cell apoptosis. Each experiment was conducted in triplicate. Error bars represent the mean ± SEM. *** $p < 0.001$, **** $p < 0.0001$; ns, not significant.

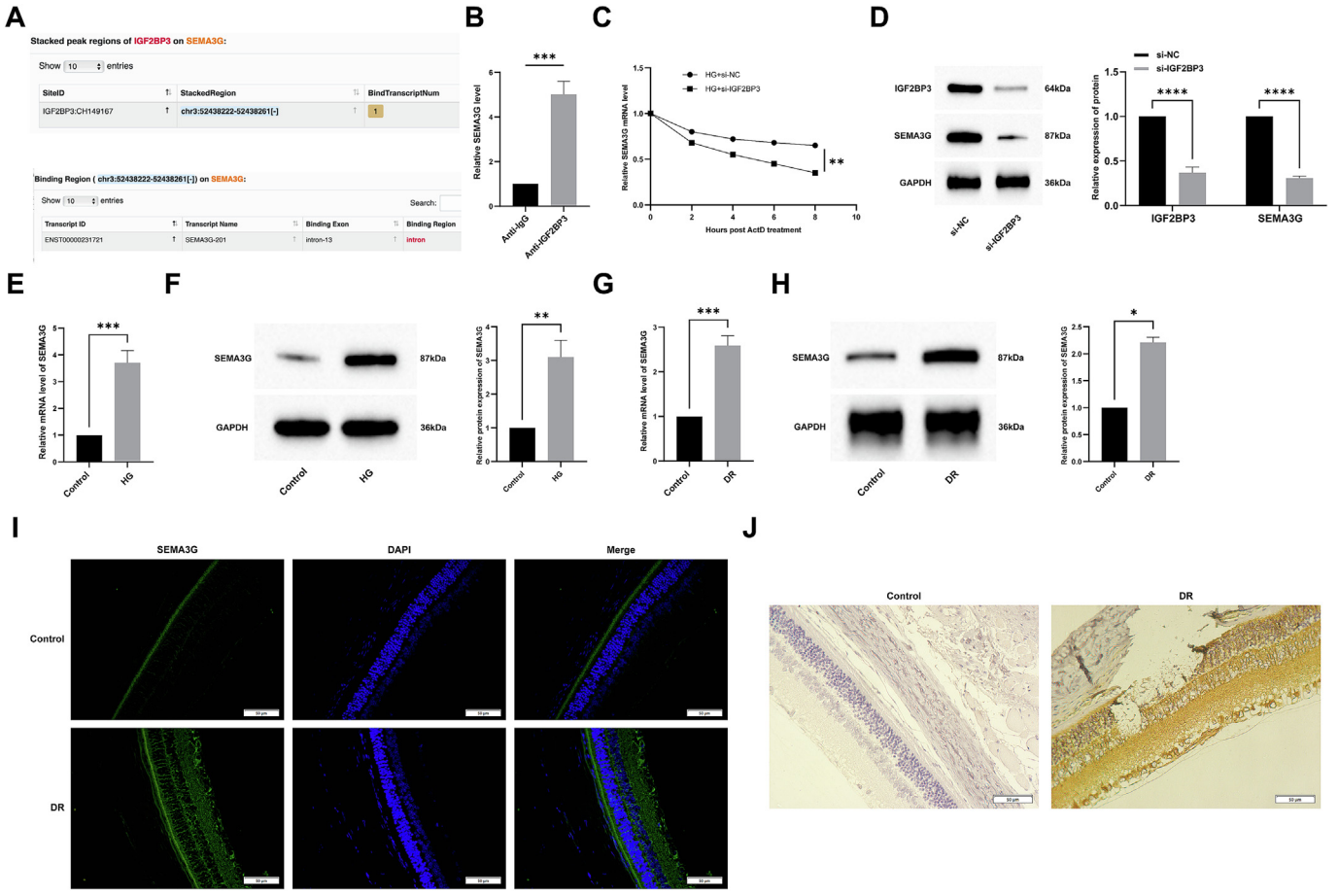

Fig. 4. Elevated SEMA3G expression in DR mediated by IGF2BP3-dependent mRNA stabilization. (A) StarBase 3.0 prediction of IGF2BP3 binding sites with SEMA3G; (B) RIP assay detecting SEMA3G mRNA levels in HRMECs; (C) SEMA3G mRNA levels following actinomycin D treatment; (D) Western blot analysis of IGF2BP3-mediated regulation of SEMA3G expression; (E) RT-qPCR analysis of differential SEMA3G mRNA expression in DR cells; (F) Western blot analysis of differential SEMA3G protein expression in DR cells; (G) RT-qPCR measurement of SEMA3G mRNA expression in retinal tissues of DR animals; (H) Western blot analysis of SEMA3G protein expression in retinal tissues of DR animals; (I) Immunofluorescence staining of SEMA3G in controls versus DR mice. Scale bar: 50 μm; (J) Immunohistochemical staining of SEMA3G in controls versus DR mice. Scale bar: 50 μm. Error bars represent the mean ± SEM. * $p < 0.05$; ** $p < 0.01$; *** $p < 0.001$; **** $p < 0.0001$; ns, not significant.

significantly reduced upon IGF2BP3 knockdown (Fig. 4C). Consistently, SEMA3G mRNA and protein levels were markedly decreased in IGF2BP3-depleted HRMECs (Fig. 4D, Fig. S1B), suggesting that IGF2BP3 enhances SEMA3G expression by stabilizing its mRNA at the post-transcriptional level. Additionally, RT-qPCR and Western blot analysis revealed elevated SEMA3G expression in DR cellular models (Fig. 4E, F, Fig. S1C). Similarly, increased SEMA3G mRNA and protein levels were observed in DR mice (Fig. 4G, H). Immunofluorescence and immunohistochemistry further confirmed the upregulation of SEMA3G in DR (Fig. 4I, J). These findings not only validate the overexpression of SEMA3G in DR but also support the potential role of IGF2BP3 in modulating SEMA3G mRNA stability during DR progression.

3.5. Knockdown of SEMA3G exhibits similar effects to IGF2BP3 knockdown on cell migration, proliferation and angiogenesis

To investigate SEMA3G's functional significance in HRMECs, gene-specific silencing was achieved using a designed siRNA. Knockdown efficiency was validated at both transcriptional and translational levels through RT-qPCR and immunoblotting analyses (Fig. 5A, B). Cellular migration capacity showed significant attenuation following SEMA3G depletion, as quantified by wound closure assays (Fig. 5C). Assessment of proliferative activity using CCK-8 and EdU incorporation methods revealed substantial growth inhibition in SEMA3G-deficient cells (Fig. 5D, E). Immunoblot analysis detected marked downregulation of cyclin D1, a critical cell cycle regulator, in silenced populations (Fig. 5F). *In vitro* angiogenesis evaluation demonstrated severely compromised tube-forming capability in SEMA3G-knockdown HRMECs (Fig. 5G), accompanied by reduced expression of angiogenesis-related proteins (Fig. 5H). These collective findings establish SEMA3G as a key mediator of vascular endothelial cell function, influencing multiple aspects of angiogenesis and vascular remodeling through protein-level regulatory mechanisms.

3.6. Overexpression of SEMA3G attenuates IGF2BP3 knockdown-mediated suppression of DR development

To assess whether the overexpression of SEMA3G could mitigate the effects of IGF2BP3 knockdown on DR development, a series of functional experiments were conducted. Wound healing assays revealed that the diminished migratory capacity observed in IGF2BP3-deficient HRMECs was effectively restored with SEMA3G overexpression (Fig. 6A, B). Consistent with these observations, flow cytometry analysis indicated that the increased apoptosis rate resulting from IGF2BP3 silencing was significantly reduced following SEMA3G overexpression (Fig. 6D). However, the elevated expression of pro-inflammatory cytokines, including TNF-α, IL-1β, IL-6, and MCP-1, observed upon IGF2BP3 knockdown

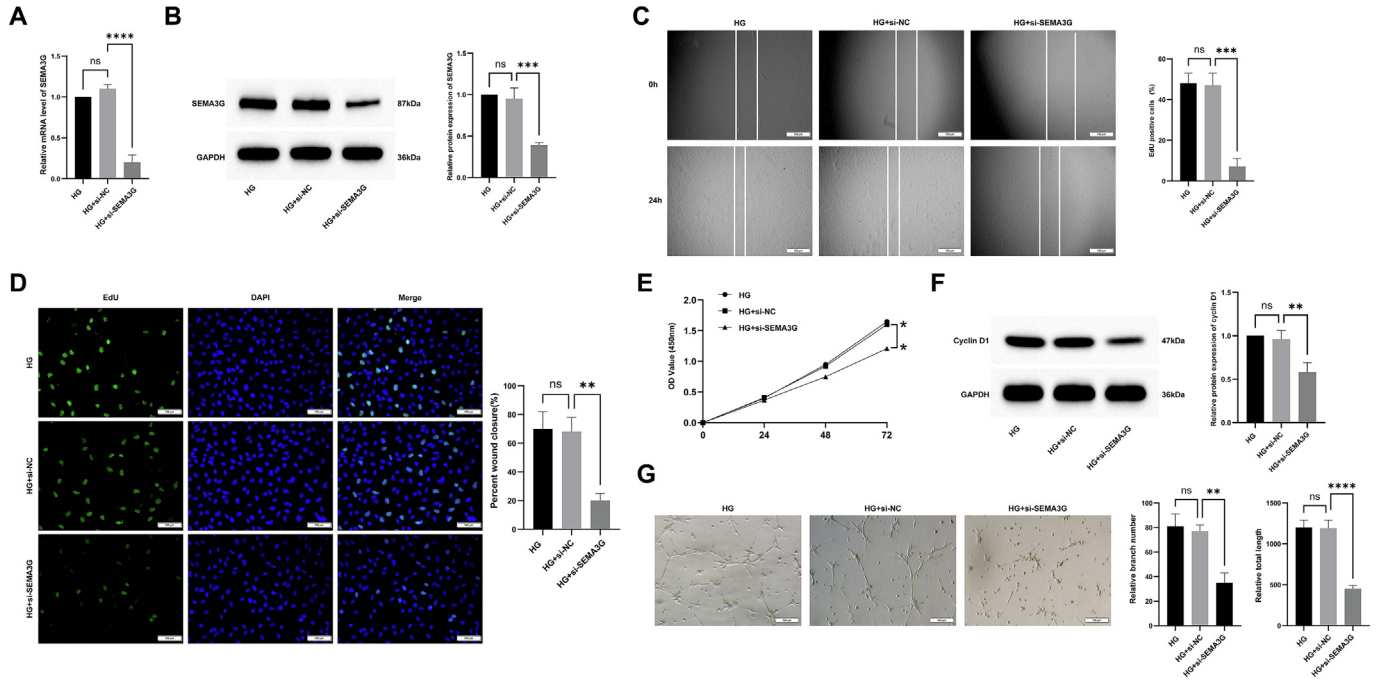

Fig. 5. The effects of SEMA3G on cell migration, proliferation and angiogenesis. (A) RT-qPCR analysis of si-SEMA3G transfection efficiency; (B) Western blot analysis of SEMA3G transfection efficiency; (C) Wound healing assay evaluating cell migration after si-SEMA3G treatment. Scale bar: 100 μm; (D) EdU assay assessing the effect of si-SEMA3G on cell proliferation. Scale bar: 100 μm; (E) CCK-8 assay measuring the effect of si-SEMA3G on cell proliferation; (F) Western blot analysis of cyclin D1 protein levels following si-SEMA3G transfection; (G) Tube formation assay examining the effects of HG and si-SEMA3G on HRMEC angiogenic capacity. Scale bar: 100 μm. Error bars represent mean ± SEM. ** $p < 0.01$; *** $p < 0.001$; **** $p < 0.0001$; ns, not significant.

remained largely unaffected by SEMA3G overexpression (Fig. 6C). These observations suggest that SEMA3G can partially reverse the pathological effects induced by IGF2BP3 deficiency, particularly by restoring cell migration and reducing apoptosis, but not by modulating the inflammatory response associated with DR development.

3.7. Overexpression of IGF2BP3 significantly accelerates DR development in vivo

Immunofluorescence and immunohistochemistry analyses (Fig. 7A, B) revealed a significant reduction in IGF2BP3 expression in the AAV-sh-IGF2BP3 group compared to the AAV-sh-NC group. Conversely, IGF2BP3 expression was notably elevated in the AAV-oe-IGF2BP3 group relative to the AAV-oe-NC group, confirming the successful modulation of gene expression by viral delivery in the DR mouse model. Histological examination using HE staining (Fig. 7C) demonstrated that retinal cells in DR mice injected with either AAV-oe-NC or AAV-sh-NC were irregularly arranged, with some areas showing cell loss or blurred structures. In contrast, the retina of mice in the AAV-sh-IGF2BP3 group exhibited a more organized and tightly packed structure, with no apparent tissue damage. Additionally, the thickness of the whole retina, as well as the inner and outer nuclear layers, was significantly increased, with no signs of neovascularization. However, in the AAV-oe-IGF2BP3 group, neovascularization was evident in the inner nuclear layer, and the outer nuclear layer showed a more disorganized structure with increased pathological changes compared to the other groups. Western blot analysis (Fig. 7D, E) further supported these findings, showing a significant decrease in the expression of CD31, VEGFA, and cyclin D1 in the AAV-sh-IGF2BP3 group, while these protein levels were markedly elevated in the AAV-oe-IGF2BP3 group. Collectively, these *in vivo* results suggest that overexpression of IGF2BP3 contributes to the exacerbation of DR development.

4. Discussion

DR, one of the most prevalent diabetic complications, remains a leading cause of vision impairment and blindness globally [19]. Diabetes influences several eye structures, but its primary pathological changes are found in the retinal blood vessels [20]. As the most prevalent microvascular complication associated with diabetes, DR is characterized by endothelial dysfunction, disruption of the blood-retinal barrier, retinal ischemia and hypoxia, and pathological neovascularization [21]. Current therapeutic interventions for advanced stages of DR, such as anti-VEGF therapy, laser photocoagulation, and vitrectomy, frequently result in suboptimal outcomes and are associated with significant side effects [22,23]. These clinical challenges highlight the pressing necessity to elucidate the molecular mechanisms governing angiogenic factors, which could lead to the development of innovative therapeutic strategies for DR. This study has identified IGF2BP3 and its downstream target, SEMA3G, as pivotal regulators in the progression of DR. IGF2BP3 facilitates DR pathogenesis by stabilizing SEMA3G mRNA.

IGF2BP3, a highly conserved member of the IGF2BP family, is an RBP that exhibits specific high expression during embryogenesis and aberrant reactivation in adulthood, during which it promotes oncogenic effects [24]. It regulates diverse physiological and pathological processes, particularly in tumor onset and progression [25]. Emerging evidence indicates that IGF2BP3 upregulation not only contributes to tumorigenesis but also disrupts glucose metabolism by inducing insulin resistance and β-cell dysfunction, thereby exacerbating type 2 diabetes progression [26]. Additionally, IGF2BP3 overexpression has been detected in ocular malignancies [27], suggesting potential ocular pathological roles. It was found that IGF2BP3 expression was significantly upregulated in the vitreous humor of patients with DR, as well as in the HG-induced HRMEC model and the retinas of diabetic mice. Mechanistically, IGF2BP3 recognizes and stabilizes m^{6}A-modified VEGFA mRNA,

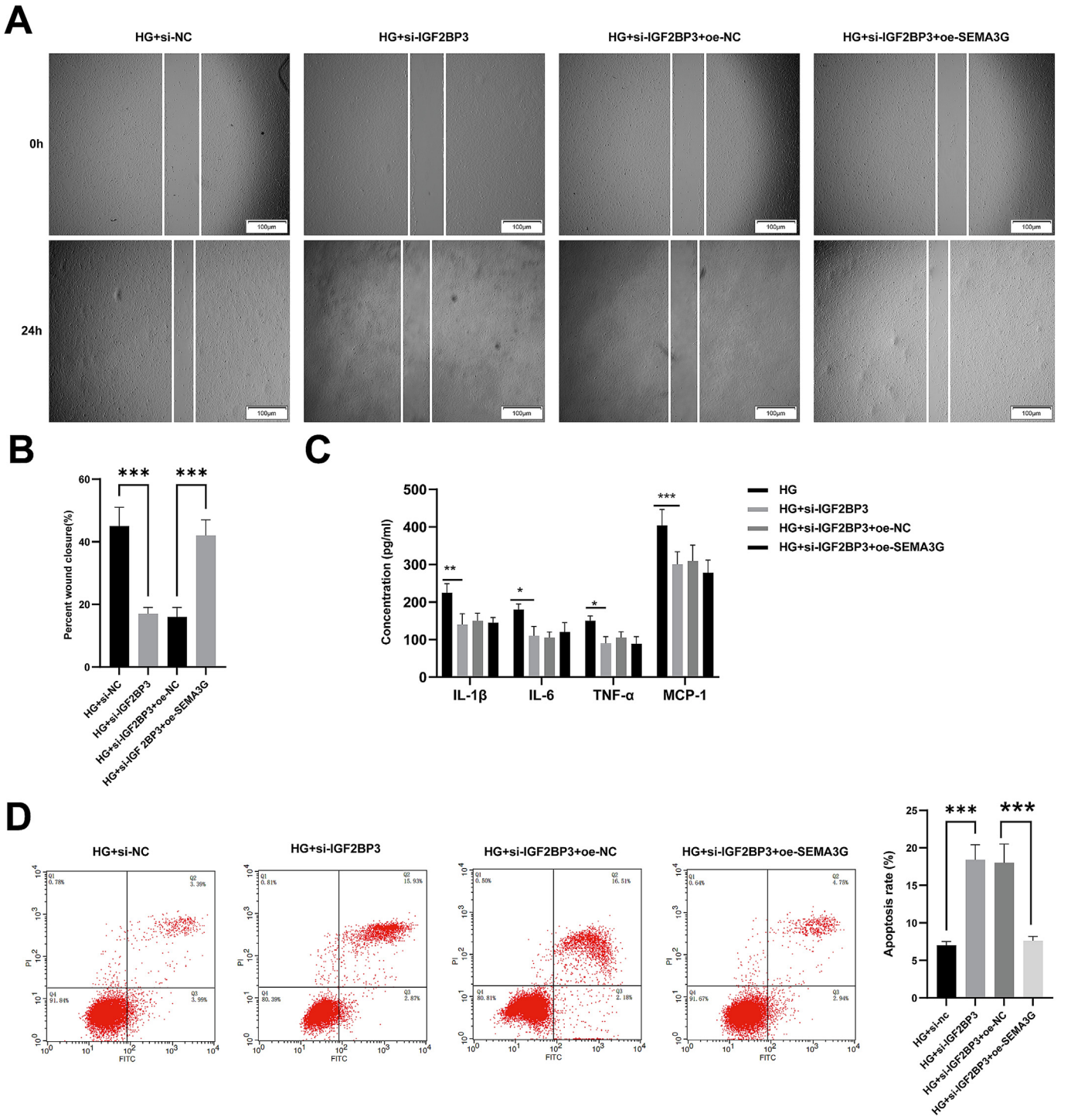

Fig. 6. Overexpression of SEMA3G attenuates the suppressive effect of IGF2BP3 knockdown on HRMEC migration. (A, B) Wound healing assay assessing cell migration capacity following transfection with si-IGF2BP3 and/or OE-SEMA3G. Scale bar: 100 μm; (C) ELISA measurement of TNF-α, IL-1β, IL-6, and MCP-1 levels; (D) Flow cytometry analysis of cell apoptosis. Error bars represent mean ± SEM. * $p < 0.05$, ** $p < 0.01$, *** $p < 0.001$, ns, not significant.

enhancing angiogenesis in HUVECs [28]. Knockdown of IGF2BP3 has been shown to interfere with colon cancer angiogenesis by disrupting VEGFA mRNA expression and stability [29]. Consistently, it was observed that IGF2BP3 knockdown in HRMECs reduced VEGFA expression and impaired angiogenic capacity. Furthermore, IGF2BP3 promotes tumor progression by stabilizing oncogenic transcripts (e.g., MYC) and exacerbates inflammation in hyperglycemic conditions [30]. In this study, an HG-induced injury model utilizing HRMECs was developed to examine the role of IGF2BP3. The findings revealed that the silencing of IGF2BP3 resulted in a substantial decrease in the expression levels of Cyclin D1 and CD31, along with a notable reduction in cellular migratory capacity. Additionally, IGF2BP3 knockdown was correlated with increased levels of inflammatory cytokines and a heightened rate of apoptosis. *In vivo* experiments further corroborated these results, demonstrating that IGF2BP3 overexpression in a DR mouse model exacerbated retinal injury and promoted pathological microvascular formation. Collectively, these findings suggest that

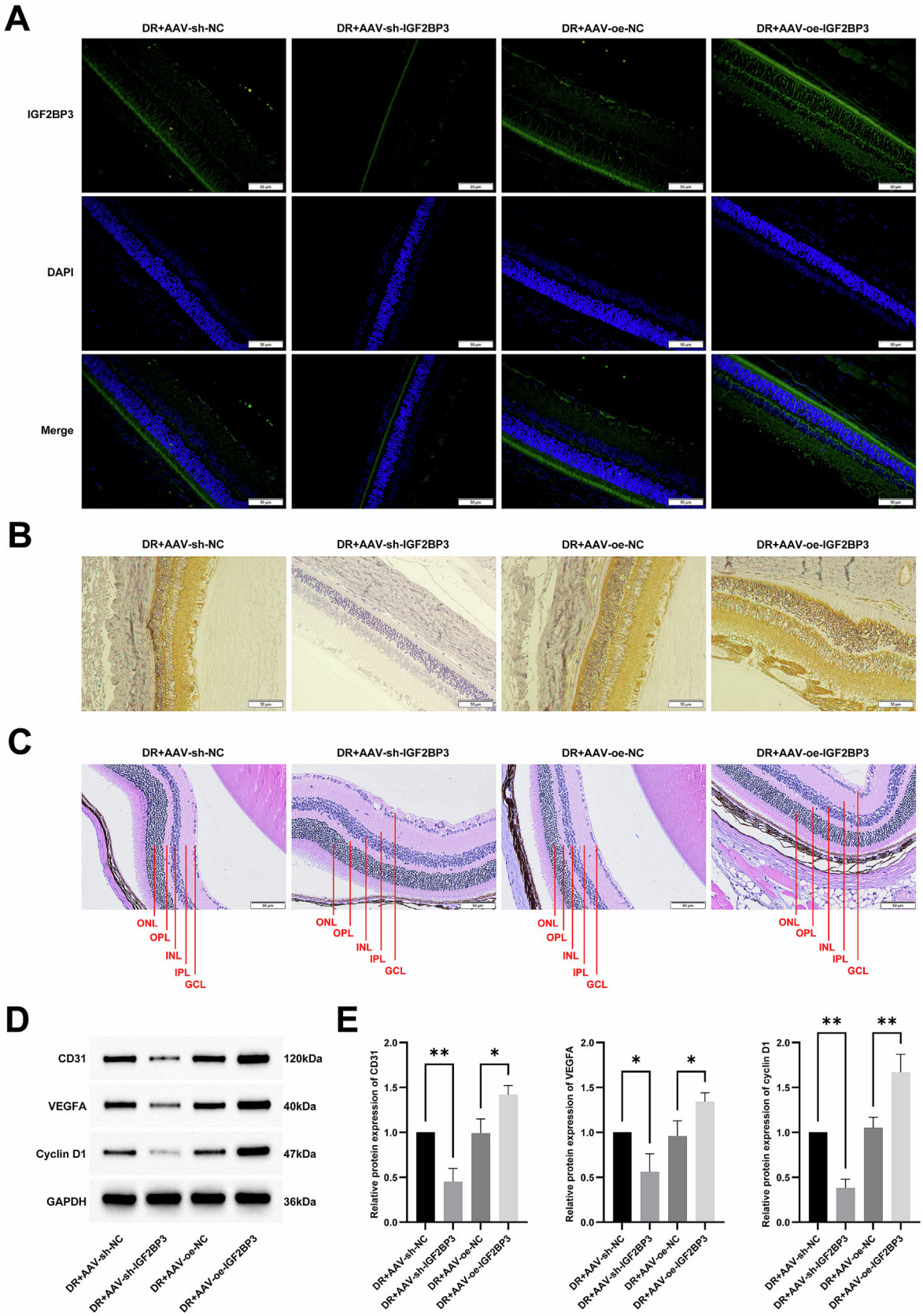

Fig. 7. Overexpression of IGF2BP3 significantly accelerates DR development *in vivo*. (A) Immunofluorescence of IGF2BP3 in DR mice following intravitreal injection of AAV-sh-NC, AAV-sh-IGF2BP3, AAV-oe-NC, or AAV-oe-IGF2BP3. Scale bar: 50 μm; (B) Immunohistochemical staining of IGF2BP3 in DR mice after intravitreal injection of AAV-sh-NC, AAV-sh-IGF2BP3, AAV-oe-NC, or AAV-oe-IGF2BP3. Scale bar: 50 μm; (C) Representative HE-stained images of DR mice intravitreally injected with AAV-sh-NC, AAV-sh-IGF2BP3, AAV-oe-NC, or AAV-oe-IGF2BP3. Scale bar: 50 μm; (D, E) Western blot analysis of CD31, VEGFA, and Cyclin D1 protein expression following transfection with AAV-sh-NC, AAV-sh-IGF2BP3, AAV-oe-NC, or AAV-oe-IGF2BP3. Error bars represent mean ± SEM. * $p < 0.05$, ** $p < 0.01$. GCL, ganglion cell layer; IPL, inner plexiform layer; INL, inner nuclear layer; OPL, outer plexiform layer; ONL, outer nuclear layer.

IGF2BP3 plays a critical role in the progression of DR by facilitating endothelial dysfunction, inflammation, and neovascularization.

IGF2BP3, an RBP, critically regulates physiological and pathological processes through mRNA stabilization. In myocardial repair, IGF2BP3 enhances cardiac regeneration by stabilizing m^6A-modified matrix metalloproteinase 3 mRNA [31]. Similarly, in rheumatoid arthritis, its homolog IGF2BP1 promotes synovial invasion through citrullination-dependent stabilization of SEMA3D mRNA [32]. These findings suggest that IGF2BP family proteins may participate in disease progression through conserved RNA stability regulatory mechanisms. In this study, bioinformatics analysis and experimental validation identified SEMA3G as a key downstream target of IGF2BP3 in DR. The data showed that SEMA3G was highly expressed in DR and promoted angiogenesis, consistent with a previous study by Chen et al. [14], which reported elevated SEMA3G expression in the vitreous humor of proliferative diabetic retinopathy (PDR) patients. The study by Chen et al. [14] also indicated that increased SEMA3G expression in PDR patients' vitreous humor could regulate physiological blood vessel remodeling. RIP and mRNA stability assays confirmed that IGF2BP3 directly binds to SEMA3G mRNA and enhances its stability. Further investigation revealed that overexpression of SEMA3G partially reversed the effects of IGF2BP3 knockdown on cell migration and apoptosis, but did not restore the levels of inflammatory cytokines. This suggests that SEMA3G mainly mediates angiogenesis and cell survival pathways. Previous studies have shown that SEMA3G inhibits VEGF-induced VEGF receptor type-2 phosphorylation, thereby impeding pulmonary artery endothelial cell migration and angiogenesis [13]. Therefore, the inhibitory effects of si-SEMA3G on HRMEC migration and angiogenesis may be mediated through the suppression of VEGF expression. Notably, overexpression of SEMA3G did not reverse the inhibitory effect of IGF2BP3 knockdown on inflammatory cytokines, suggesting that the inflammation regulation may depend on other IGF2BP3 target genes [33–35].

However, there are limitations to this study. First, the use of HRMECs alone does not fully reflect the roles of other retinal cell types (e.g., pericytes, glial cells). The mechanistic study failed to confirm the m^6A modification of SEMA3G mRNA and its effect on IGF2BP3 binding, and it also did not clarify the downstream signaling pathways. Finally, in terms of clinical cohort design, idiopathic macular holes were selected as the control group for comparison with the progressive PDR group. However, due to the absence of a non-proliferative diabetic retinopathy (NPDR) group, it remains unclear whether this upregulation occurs during the pre-proliferative stage or is strictly associated with the onset of the proliferative stage. Therefore, future studies should include NPDR patient samples for confirmation and introduce more detailed cellular models to further explore the relevant mechanisms.

This investigation provides comprehensive evidence supporting the pathogenic role of IGF2BP3 in DR development through post-transcriptional stabilization of SEMA3G mRNA. Clinical specimen analysis combined with experimental models revealed consistent upregulation of IGF2BP3 in DR conditions and its functional involvement in modulating SEMA3G transcript stability. Genetic inhibition of IGF2BP3 significantly impaired multiple pathological processes including vascular endothelial cell proliferation, migratory capacity, and angiogenic potential, while concurrently reducing inflammatory cytokine secretion and cellular apoptosis. The identified IGF2BP3-SEMA3G regulatory axis appears to constitute a critical molecular mechanism underlying DR pathogenesis. These results advance current understanding of DR disease mechanisms and highlight the translational potential of both IGF2BP3 and SEMA3G as candidate biomarkers and molecular targets for therapeutic intervention.

Ethical approval

The present study was approved by the Ethics Committee of China-Japan Friendship Hospital, and written informed consent was provided by all patients prior to the study start. All procedures were performed in accordance with the ethical standards of the Institutional Review Board and the Declaration of Helsinki, and its later amendments or comparable ethical standards (2020-12-K09).

All animal experiments complied with the ARRIVE guidelines and were performed in accordance with the National Institutes of Health Guide for the Care and Use of Laboratory Animals. The experiments were approved by the Institutional Animal Care and Use Committee of China-Japan Friendship Hospital (ZRDWLL240055).

Financial support

This research was supported by internal research funding of China-Japan Friendship Hospital.

CRediT authorship contribution statement

You Chen: Visualization, Supervision, Project administration, Data curation. **Tong Zhao:** Software, Project administration, Investigation, Formal analysis. **MengYu Han:** Project administration, Methodology, Funding acquisition, Formal analysis. **Yi Chen:** Visualization, Supervision, Project administration, Data curation.

Data availability

Data are available from the corresponding author on request.

Declaration of competing interest

The authors declare that they have no known competing financial interests or personal relationships that could have appeared to influence the work reported in this paper.

Supplementary material

Supplementary data to this article can be found online at https://doi.org/10.1016/j.ejbt.2026.100723.

References

[1] Genitsaridi I, Salpea P, Salim A, et al. 11th edition of the IDF Diabetes Atlas: Global, regional, and national diabetes prevalence estimates for 2024 and projections for 2050. Lancet Diabetes Endocrinol 2026;14(2):149–56. https://doi.org/10.1016/s2213-8587(25)00299-2. PMid: 41412135.
[2] Guo C, Deshpande M, Niu Y, et al. HIF-1α accumulation in response to transient hypoglycemia may worsen diabetic eye disease. Cell Rep 2023;42(1):111976. https://doi.org/10.1016/j.celrep.2022.111976. PMid: 36640318.
[3] Chong DD, Das N, Singh RP. Diabetic retinopathy: Screening, prevention, and treatment. Cleve Clin J Med 2024;91(8):503–10. https://doi.org/10.3949/ccjm.91a.24028. PMid: 39089852.
[4] Zhou Y, Xuan Y, Liu Y, et al. Transcription factor FOXP1 mediates vascular endothelial dysfunction in diabetic retinopathy. Graefe's Arch Clin Exp Ophthalmol 2022;260(12):3857–67. https://doi.org/10.1007/s00417-022-05698-3. PMid: 35695913.
[5] Wang N, Yao F, Liu D, et al. RNA N6-methyladenosine in nonocular and ocular disease. J Cell Physiol 2022;237(3):1686–710. https://doi.org/10.1002/jcp.30652. PMid: 34913163.
[6] Breier G, Chavakis T, Hirsch E. Angiogenesis in metabolic-vascular disease. Thromb Haemost 2017;117(7):1289–95. https://doi.org/10.1160/th17-05-0325. PMid: 28594427.
[7] Wang S, Park JK, Duh EJ. Novel targets against retinal angiogenesis in diabetic retinopathy. Curr Diab Rep 2012;12(4):355–63. https://doi.org/10.1007/s11892-012-0289-0. PMid: 22638940.

[8] Huang W, Li Y, Zhang C, et al. IGF2BP3 facilitates cell proliferation and tumorigenesis via modulation of JAK/STAT signalling pathway in human bladder cancer. J Cell Mol Med 2020;24(23):13949–60. https://doi.org/10.1111/jcmm.16003. PMid: 33094561.
[9] Tian Y, Cheng W, Wang H, et al. Ascorbic acid protects retinal pigment epithelial cells from high glucose by inhibiting the NF-κB signal pathway through MALAT1/IGF2BP3 axis. Diabetic Med 2023;40(5):e15050. https://doi.org/10.1111/dme.15050. PMid: 36661363.
[10] Sakurai A, Doçi CL, Gutkind JS. Semaphorin signaling in angiogenesis, lymphangiogenesis and cancer. Cell Res 2012;22(1):23–32. https://doi.org/10.1038/cr.2011.198. PMid: 22157652.
[11] Tan C, Lu NN, Wang CK, et al. Endothelium-derived semaphorin 3G regulates hippocampal synaptic structure and plasticity via Neuropilin-2/PlexinA4. Neuron 2019;101(5):920–937.e13. https://doi.org/10.1016/j.neuron.2018.12.036. PMid: 30685224.
[12] Chi H, Deng S, Xu K, et al. SEMA3G-NRP1 Signaling functions as an immune checkpoint that enables tumor immune evasion by impairing T-cell cytotoxicity. Cancer Res 2025;85(5):912–24. https://doi.org/10.1158/0008-5472.Can-24-2223. PMid: 39652581.
[13] Mirza SL, Upton PD, Hodgson J, et al. SEMA3G regulates BMP9 inhibition of VEGF-mediated migration and network formation in pulmonary endothelial cells. Vasc Pharmacol 2024;155:107381. https://doi.org/10.1016/j.vph.2024.107381. PMid: 38795838.
[14] Chen DY, Sun NH, Chen X, et al. Endothelium-derived semaphorin 3G attenuates ischemic retinopathy by coordinating β-catenin-dependent vascular remodeling. J Clin Investig 2021;131(4):e135296. https://doi.org/10.1172/jci135296. PMid: 33586674.
[15] Hyun J, Lee M, Rehman J, et al. Notch1 promotes ordered revascularization through Semaphorin 3g modulation of downstream vascular patterning signalling factors. J Physiol 2022;600(3):509–30. https://doi.org/10.1113/jp282286. PMid: 34921404.
[16] Luo XY, Fu X, Liu F, et al. Sema3G activates YAP and promotes VSMCs proliferation and migration via Nrp2/PlexinA1. Cell Signal 2023;105:110613. https://doi.org/10.1016/j.cellsig.2023.110613. PMid: 36720439.
[17] Lv L, Wei Q, Zhang J, et al. IGF2BP3 prevent HMGB1 mRNA decay in bladder cancer and development. Cell Mol Biol Lett 2024;29(1):39. https://doi.org/10.1186/s11658-024-00545-1. PMid: 38504159.
[18] Wang R, Xue W, Kan F, et al. NSUN2 affects diabetic retinopathy progression by regulating MUC1 expression through RNA m^5C methylation. J Transl Med 2024;22(1):476. https://doi.org/10.1186/s12967-024-05287-4. PMid: 38764010.
[19] Ogurtsova K, da Rocha Fernandes JD, Huang Y, et al. IDF Diabetes Atlas: Global estimates for the prevalence of diabetes for 2015 and 2040. Diabetes ResClin Pract 2017;128:40–50. https://doi.org/10.1016/j.diabres.2017.03.024. PMid: 28437734.
[20] Antonetti DA, Silva PS, Stitt AW. Publisher correction: Current understanding of the molecular and cellular pathology of diabetic retinopathy. Nat RevEndocrinol 2025;21(1):62. https://doi.org/10.1038/s41574-024-01053-0. PMid: 39448833.
[21] Abu El-Asrar AM, Nawaz MI, Ahmad A, et al. CD40 Ligand-CD40 interaction is an intermediary between inflammation and angiogenesis in proliferative diabetic retinopathy. Int J Mol Sci 2023;24(21):15582. https://doi.org/10.3390/ijms242115582. PMid: 37958563.
[22] Madjedi K, Pereira A, Ballios BG, et al. Switching between anti-VEGF agents in the management of refractory diabetic macular edema: A systematic review. Surv Ophthalmol 2022;67(5):1364–72. https://doi.org/10.1016/j.survophthal.2022.04.001. PMid: 35452685.
[23] Xue L, Hu M, Zhu Q, et al. GRg1 inhibits the TLR4/NF-kB signaling pathway by upregulating miR-216a-5p to reduce growth factors and inflammatory cytokines in DR. Mol Biol Rep 2023;50(11):9379–94. https://doi.org/10.1007/s11033-023-08895-3. PMid: 37819496.
[24] Bell JL, Wächter K, Mühleck B, et al. Insulin-like growth factor 2 mRNA-binding proteins (IGF2BPs): Post-transcriptional drivers of cancer progression? Cell Mol Life Sci 2013;70(15):2657–75. https://doi.org/10.1007/s00018-012-1186-z. PMid: 23069990.
[25] Mancarella C, Scotlandi K. IGF2BP3 from physiology to cancer: Novel discoveries, unsolved issues, and future perspectives. Front Cell Dev Biol 2020;7:363. https://doi.org/10.3389/fcell.2019.00363. PMid: 32010687.
[26] Rattanapan Y, Nongwa K, Supanpong C, et al. Downregulation of *miR-25-3p* and its impact on *PTAFR* and *IGF2BP3* expression in type 2 diabetes mellitus: Implications for biomarker discovery and disease pathogenesis. J Clin Med Res 2024;16(11):536–46. https://doi.org/10.14740/jocmr6099. PMid: 39635336.
[27] Wan Q, Tang J. Exploration of potential key pathways and genes in multiple ocular cancers through bioinformatics analysis. Graefes Arch Clin Exp Ophthalmol 2019;257(10):2329–41. https://doi.org/10.1007/s00417-019-04410-2. PMid: 31309275.
[28] Xu X, Wu S, Zhang Y, et al. m6A modification of VEGFA mRNA by RBM15/YTHDF2/IGF2BP3 contributes to angiogenesis of hepatocellular carcinoma. Mol Carcinog 2024;63(11):2174–89. https://doi.org/10.1002/mc.23802. PMid: 39092767.
[29] Huang H, Weng H, Sun W, et al. Recognition of RNA N^6-methyladenosine by IGF2BP proteins enhances mRNA stability and translation. Nat Cell Biol 2018;20(3):285–95. https://doi.org/10.1038/s41556-018-0045-zv. PMid: 29476152.
[30] Tian Y, Cheng W, Wang H, et al. Ascorbic acid protects retinal pigment epithelial cells from high glucose by inhibiting the NF-κB signal pathway through MALAT1/IGF2BP3 axis. Diabetic Med 2023;40(5):e15050. https://doi.org/10.1111/dme.15050. PMid: 36661363.
[31] Li S, Shen S, Xu H, et al. IGF2BP3 promotes adult myocardial regeneration by stabilizing *MMP3* mRNA through interaction with m6A modification. Cell Death & Discovery 2023;9(1):164. https://doi.org/10.1038/s41420-023-01457-3. PMid: 37188676.
[32] Qin Y, Liu L, Zhang Y, et al. Citrullinated IGF2BP1 promotes rheumatoid synovial aggression via increasing the mRNA stability of SEMA3D. Commun Biol 2025;8(1):50. https://doi.org/10.1038/s42003-025-07492-3. PMid: 39809921.
[33] Zhao H, Wang Y, Liang C, et al. LncRNA FOXD3-AS1/miR-128-3p axis-mediated IGF2BP3 in glioma stimulates cancer angiogenesis and progression. Folia Neuropathol 2023;61(2):168–84. https://doi.org/10.5114/fn.2023.126862. PMid: 37587892.
[34] Hou D, Zhao W, Yang Q, et al. Curcumol promotes immune cell invasion and inhibits angiogenesis in colon cancer by decreasing IGF2BP3 expression. Biochem Biophys Res Commun 2025;750:151394. https://doi.org/10.1016/j.bbrc.2025.151394. PMid: 39899937.
[35] Xu M, Guo Y, Wang F, et al. Enterolactone combined with m6A Reader IGF2BP3 inhibits malignant angiogenesis and disease progression in ovarian cancer. Phytomedicine 2025;136:156343. https://doi.org/10.1016/j.phymed.2024.156343. PMid: 39765033.